Supplemental Materials

Genotype (*Nrarp*)	Cervical	Thoracic	Lumbar	Sacral	Lumbar + Sacral
+/+	7	13	6	4	10
+/+	7	13	6	4	10
+/+	7	13	6	4	10
+/+	7	13	6	4	10
+/+	7	13	6	4	10
+/+	7	13	6	4	10
+/+	7	13	6	4	10
+/+	7	13	6	4	10
+/+	7	13	6	4	10
+/+	7	13	6	4	10
+/+	7	13	5	5	10
-/-	7	13	5	4	9
-/-	7	13	5	4	9
-/-	7	13	5	4	9
-/-	7	13	5	4	9
-/-	7	13	5	4	9
-/-	7	13	5	4	9
-/-	7	13	5	4	9
-/-	7	13	5	5	10

Table S1. The number of vertebrae in newborn mice.

The numbers of vertebrae in the newborn mice were counted after the mice were stained.

Gene Symbol	Gene_Name	Probe ID	Cluster	Ratio1	Ratio2	Ratio3	Avg.
Nrarp	Notch-regulated ankyrin repeat protein	315756		0.04	0.10	0.05	0.06
Hes5	hairy and enhancer of split 5 (Drosophila)	562022		4.56	4.77	3.51	4.20
Lfng	lunatic fringe gene homolog (Drosophila)	882835		1.37	1.43	1.10	1.28
Hes7	hairy and enhancer of split 7 (Drosophila)	558449	Notch	1.18	1.20	0.57	0.87
Hes1	hairy and enhancer of split 1 (Drosophila)	406680		1.20	0.91	0.53	0.79
Hey1	hairy/enhancer-of-split related with YRPW motif 1	814590		1.55	1.13	1.32	1.31
Nkd1	naked cuticle 1 homolog (Drosophila)	394939		1.04	1.20	1.10	1.11
Axin2	axin2	357287		1.19	1.19	0.62	0.91
Lef1	lymphoid enhancer binding factor 1	928212	Wnt	1.18	1.20	1.05	1.14
Msgn1	mesogenin 1	733438		1.00	0.88	1.53	1.08
T	brachyury	661161		0.89	0.77	1.03	0.88
Dusp1	dual specificity phosphatase 1	303843		1.05	0.89	1.07	1.00
Dusp4	dual specificity phosphatase 4	672437		0.99	0.84	1.11	0.97
Dusp6	dual specificity phosphatase 6	932169	FGF	0.97	0.70	0.75	0.79
Spry2	sprouty homolog 2 (Drosophila)	872375		0.90	0.68	1.12	0.87
Spry4	sprouty homolog 4 (Drosophila)	529472		1.00	0.95	0.74	0.88
Rhox5	reproductive homeobox on X chromosome, 5	535766		3.60	2.50	2.15	2.63
Car4	carbonic anhydrase 4	349705	-*	2.42	2.11	2.30	2.27
Gpr133	G protein-coupled receptor 133	716011		2.22	2.67	2.06	2.29

Table S2. Summary of microarray analysis results.

Several target genes of the Notch, Wnt, and FGF signaling pathways are displayed. The ratios of the expression levels (*Nrarp*$^{-/-}$ / wild type) were calculated using normalized signal intensities (n = 3). *, Genes that had a more than two-fold difference for all three analyses. The functions in the segmentation clock remain unclear.

Individual no.	Cervical	Thoracic	Lumbar	Sacral	Lumbar+Sacral
1	7	13	5	5	10
2	7	13	6	4	10
3	7	13	6	5	11
4	7	13	7	4	11
5	7	13	6	4	10
6	7	13	7	4	11
7	7	13	7	4	11
8	7	13	6	4	10
9	7	13	7	4	11
10	7	13	6	4	10
11	7	13	6	4	10
	7.0 ± 0.0	13.0 ±0.0	6.3 ± 0.18	4.2 ± 0.12	10.5 ± 0.15

Table S3. Number of vertebrae in gamma-secretase inhibitor-treated mice.

An inhibitor, 0.1 mg/kg of LY411,575, was administered three times from E 7.5 to E 9.5, and the animals were then sacrificed on postnatal day 1 to prepare skeletal sample (mean ± s.e.m.).

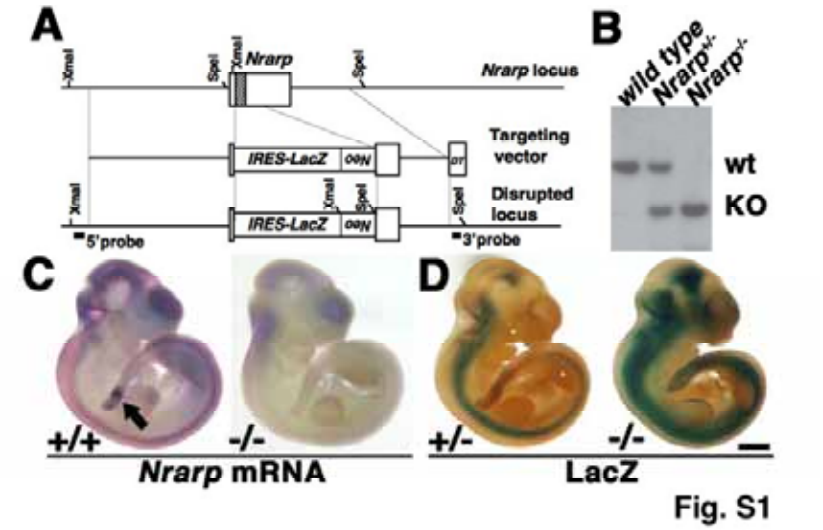

Fig. S1

Figure S1. Generation of *Nrarp*-deficient mice.

(A) Targeting strategy. The whole coding region of *Nrarp* was replaced by IRES-*LacZ* and PGK-*neo* (inverted orientation). (B) Southern blot analysis. The 3'-external probe was used to detect 6.6-kb (wild-type) and 4.5-kb (mutant) fragments in *Spe*I-digested genomic DNA. wt, wild-type; KO, knockout. (C) Whole-mount *in situ* hybridization for *Nrarp* at E 10.5. Expression was observed in the central nervous systems and the PSM (left, arrow) of wild-type embryos. In *Nrarp*$^{-/-}$ embryos, *Nrarp* expression was completely absent (right). (D) β-galactosidase activity was detected in the regions where *Nrarp* was expressed. Scale bar, 1mm.

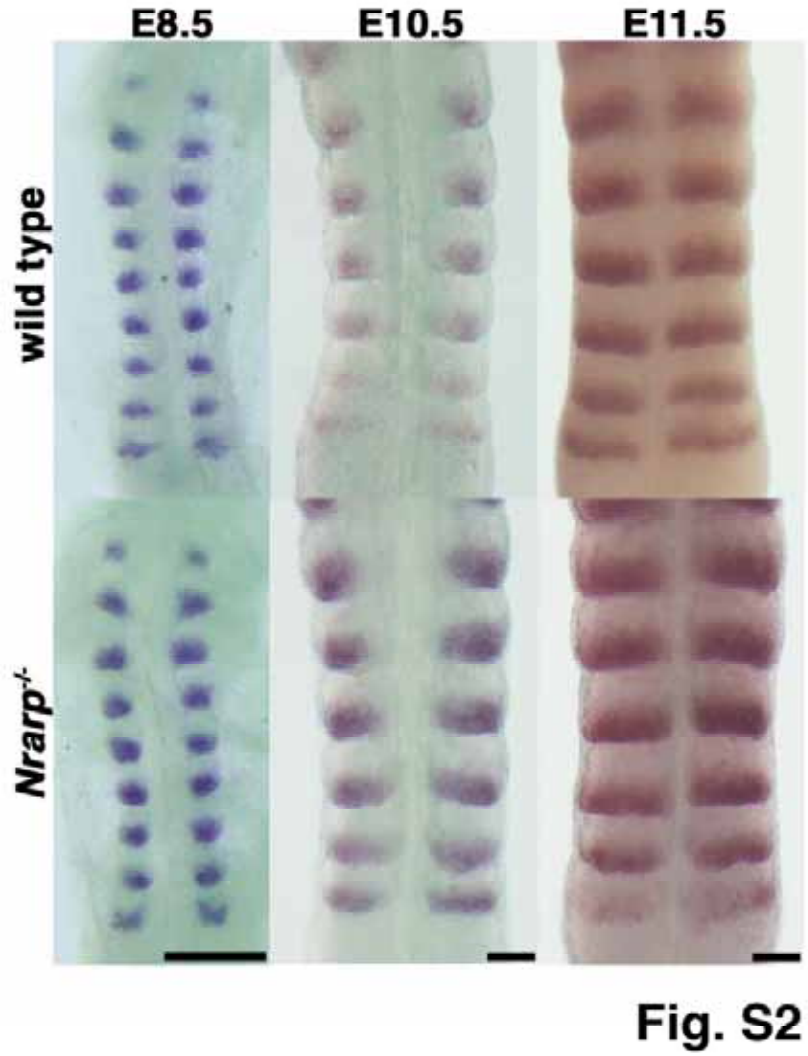

Figure S2. The shape and size of somites are not affected in *Nrarp*$^{-/-}$.

Whole-mount *in situ* hybridization for *Uncx4.1* at the indicated stages. Dorsal views of caudal part of embryos are presented. There were no significant differences in shape, symmetry, and polarity of somites between the wild-type embryos and the *Nrarp*$^{-/-}$ embryos. The top side is the anterior region. Scale bars, 500 μm.

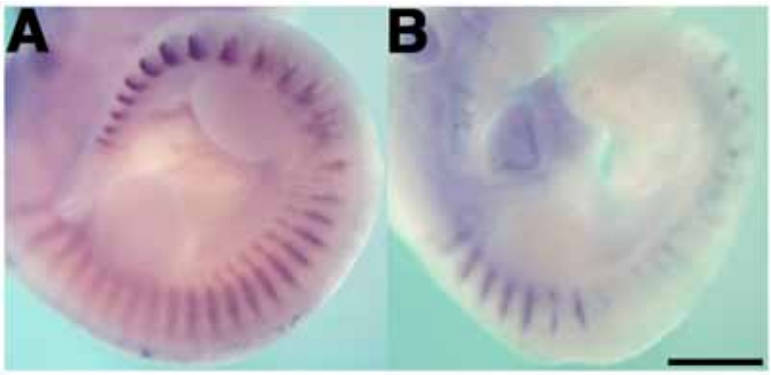

Figure S3. Notch signaling inhibition disrupts somitegenesis. Whole-mount *in situ* hybridization for *Uncx4.1* of embryos that were treated with 0.3 mg/kg LY411,575 (A) or 1.0 mg/kg LY411,575 (B). Defects were observed in somite segmentation and somite patterning (A) and in general development under high dose of inhibitor (B). Scale bars, 1 mm.

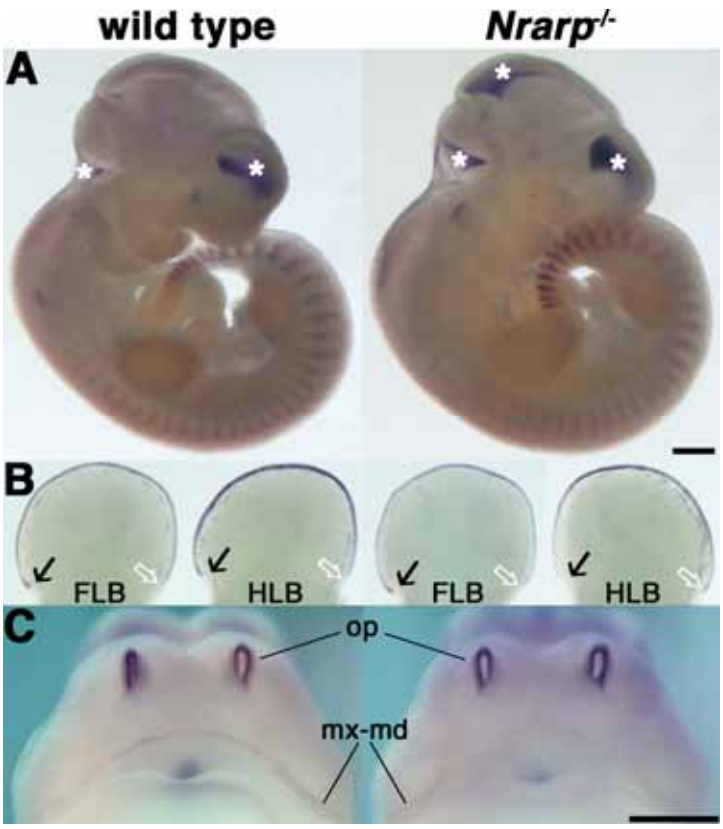

Figure S4. Pace of general development is identical between *Nrarp* mutant embryos and wild-type littermates. (A) whole-mount *in situ* hybridization of *Uncx4.1* in E10.5 emryos. White asterisks indicate non-specific staining. (B,C) *in situ* hybridization of *Fgf8* in E11.5 embryos. (B) Lateral views of limb buds. *Fgf8* mRNA expression domain revealed the apical ectoderm ridge (AER). Anterior is towards the left. Black arrows and white arrows indicate anterior end and posterior end of *Fgf8* expression domain in the AER, respectively. Narrow bands of AER are detected identically in *Nrarp*$^{-/-}$ and their wild-type littermates. We detected no differences in morphology of limb buds and their size. (C) Frontal views of the anterior half. *Fgf8* mRNA was detected at op and mx.

Differentiation levels of these organs are observed identically between mutant and their wild-type littermates. Anterior is towards the top. FLB, forelimb bud; HLB, hind limb bud; op, olfactory pits; mx, maxillary process; md, mandibular process. Scale bars, 500 μm.

Supplementary Note 1

Mathematical analysis of the Notch activity-dependent periodicity

Basic formulation of the model

To examine the dependence of the Hes7 expression period on the Notch activity, we studied the original model developed by Lewis (*1*) by following the mathematical analysis in ref (*1*). Consider a model of two variables, protein $p(t)$ and mRNA $m(t)$, formulated as,

$$\frac{\mathrm{d}p(t)}{\mathrm{d}t} = am\left(t-T_p\right) - bp(t) \tag{S1}$$

$$\frac{\mathrm{d}m(t)}{\mathrm{d}t} = \frac{k}{1+p^2\left(t-T_m\right)/p_0^2} - cm(t) \tag{S2}$$

where a and k represent protein production rates per mRNA molecule and maximum rate of mRNA, respectively, b and c are degradation rates, p_0 is a gain parameter, and T_p and T_m are time delays for protein and mRNA generation.

If we introduce a new variable $p_{adv}(t) = p\left(t+T_p\right)$, we have

$$\frac{\mathrm{d}p_{adv}(t)}{\mathrm{d}t} = am(t) - bp_{adv}(t) \tag{S3}$$

$$\frac{\mathrm{d}m(t)}{\mathrm{d}t} = \frac{k}{1+p_{adv}^2\left(t-T\right)/p_0^2} - cm(t), \tag{S4}$$

where $T = T_m + T_p$. To discuss the qualitative characteristics of the system, we introduce dimensionless variables and parameters as follows:

$$\tau = t/T\,, \quad \beta = bT\,, \quad \gamma = cT\,, \quad \kappa = ak/bcp_0\,,$$

$$P(\tau) = bcp_{adv}(t)/ak\,, \quad M(\tau) = cm(t)/k\,,$$

where the parameters, k and p_0, which regulate mRNA production rate, are aggregated into a single parameter κ, by which we can incorporate a Notch activity level into the model. Using these notations, the ODEs are transformed as

$$\frac{1}{\beta}\frac{\mathrm{d}P(\tau)}{\mathrm{d}\tau} = -\left\{P(\tau) - M(\tau)\right\} \tag{S5}$$

$$\frac{1}{\gamma}\frac{\mathrm{d}M(\tau)}{\mathrm{d}\tau} = -\left\{M(\tau) - f\left(P\left(\tau-1\right)\right)\right\} \tag{S6}$$

$$f(x) = \frac{1}{1+(\kappa x)^2}. \tag{S7}$$

Note that β and γ are Notch-independent constants and that the variables, $P(\tau)$ and $M(\tau)$, are the protein and mRNA levels normalized by the production rates a and k, respectively. These normalizations, in which both of the $P(\tau)$ and $M(\tau)$ have a range of (0,1), allow us to evaluate the protein and mRNA levels as the production rate scale. Equations (S5) and (S6) indicate that $P(\tau)$ converges to $M(\tau)$ exponentially with the β time scale, and that $M(\tau)$ approaches to the function of $P(\tau-1)$, $f(x)$, exponentially with the γ time scale.

Notch activity-dependent oscillation amplitude

Taking an analysis similar to that in ref (*1*), if the reactions are very fast due to large β and γ (so the right sides of Eqs. (S5) and (S6) can be approximated as zero), they have two quasi-steady states, (P_{max}, M_{max}) and (P_{min}, M_{min}), which satisfy

$$P_{max} = M_{max}\ ,\ P_{min} = M_{min}\ ,$$
$$M_{max} = \frac{1}{1+(\kappa P_{min})^2}\ ,\ M_{min} = \frac{1}{1+(\kappa P_{max})^2}.$$

In the case of oscillation, where the maximum is larger than the minimum, the pair of (P_{max}, P_{min}) and (M_{max}, M_{min}) are the solutions to the quadratic equation $x^2 - x + 1/\kappa^2 = 0$. Therefore,

$$P_{max} = M_{max} = \frac{1+\sqrt{1-4/\kappa^2}}{2} \tag{S8}$$

$$P_{min} = M_{min} = \frac{1-\sqrt{1-4/\kappa^2}}{2}, \tag{S9}$$

where $2 > \kappa$ for the oscillation case (Fig. S-I).

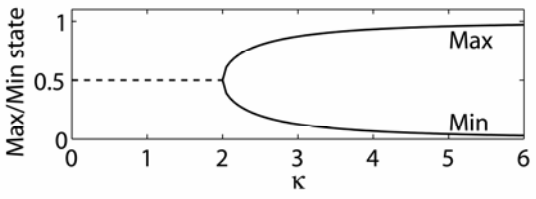

Figure S-I: Dependence of oscillation amplitude on κ corresponding to Notch activity. The maximum and minimum values of quasi-steady states described by Eq. (S8) and (S9) are shown.

Notch activity-dependent oscillation period

As analyzed in ref (*1*), the oscillation period of the model expressed as Eqs. (S5)-(S7) can be approximated as $2(T+1/\beta+1/\gamma)$ when κ changes little. If κ has a different value from a control because of experimental manipulation (*Nrarp* KO in this work), it is important to take a computational approach to examine the κ-dependent oscillation period.

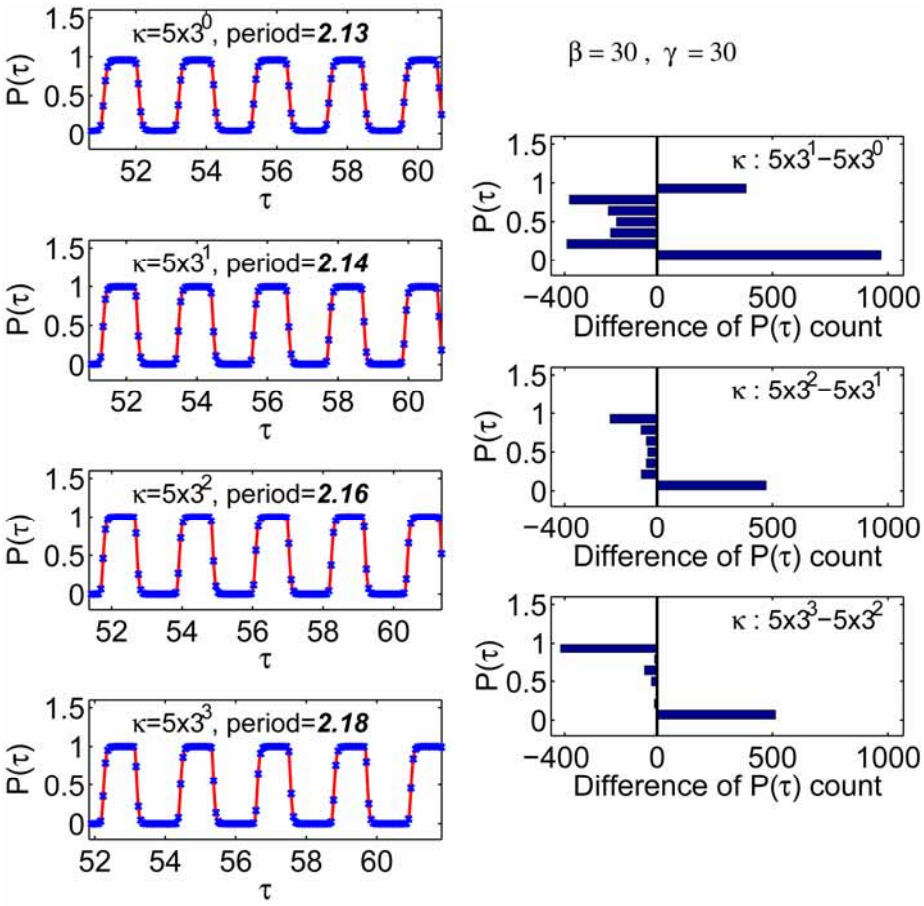

Figure S-II: Comparison of the time courses of $P(\tau)$ and the histograms of the difference between the two distributions of $P(\tau)$ (blue points on the left) obtained by two κ values for an identical calculation time (right). The values of κ and the period are shown in each figure.

The numerical simulation using Eqs. (S5)-(S7) with various κ values shows that the oscillation period has a positive correlation with κ, as shown in the left column of Fig. S-II. The figures in the right column show changes in the distribution of $P(\tau)$ values (blue points in the left column figures), suggesting that the term during which $P(\tau)$ is very small (bottom bars in the histograms) accounts for prolongation of the period by the increase in κ. Note that the period increases despite the decrease in most $P(\tau)$ values except for the bottom in the left column of

Fig. S-II. Because the parameters, T, β, and γ, are constant in the numerical calculation, only κ can contribute to prolonging of the term with small $P(\tau)$.

To discuss an approximate dependency of the period on κ, we focus on the characteristics of the function $f(x)$ defined by Eq. (S7). Figure S-III, illustrating $f(x)$, suggests that $f(x)$ becomes small if x takes on a large value, and vice versa (see Eqs. (S6) and (S7)), and it indicates that $f(x)$ is a monotonically decreasing function of x and its slope is steeper with larger κ. If we here define the threshold, S, at which the variable $f(x)$ shifts to the increasing phase when x decreases (see Fig. S-III), the very small $P(\tau)$ in the Fig. S-II is equivalent to $f(x)$ under S. Then the threshold of x in terms of S is given by

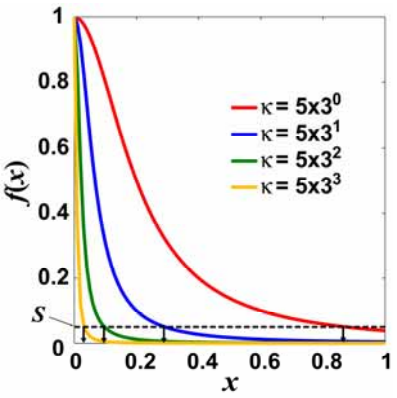

Figure S-III: Comparison of shapes of $f(x)$ with three values of the parameter κ. The horizontal dashed line indicates the threshold $f(x) = S$ at which of $f(x)$ shifts to the increasing phase when x decreases. The model oscillates when κ is larger than 2.

$$x_{th} = \frac{1}{\kappa}\sqrt{\frac{1}{S} - 1}\,. \qquad \text{(S10)}$$

When $P(\tau)$ increases by following $M(\tau)$, $P(\tau-1)$ decreases from nearly one to x_{th} according to Eqs. (S6) and (S7). Since these equations have a form of the ODE, $dx/dt = -x$, thus, the amount of the $P(\tau-1)$ decrease can be approximated by an exponential function,

$$e^{-D/\alpha} \approx \frac{1}{\kappa}\left(\frac{1}{S} - 1\right)^{1/2}, \qquad \text{(S11)}$$

where D is a time interval necessary for $P(\tau-1)$ to decrease from nearly one to x_{th} with a time constant α. By transforming this equation, we get

$$D \approx \alpha \ln \kappa - \frac{\alpha}{2}\ln\left(\frac{1}{S} - 1\right), \qquad \text{(S12)}$$

suggesting that the κ-dependent prolongation of the period has a logarithmic form of κ. This approximation shows good agreement with the numerical simulation with large κ, as shown in Fig. S-IV, where the amplitude of the oscillation is given by

$$A(\kappa) = P_{\max} - P_{\min} = \sqrt{1 - 4/\kappa^2}\,, \qquad \text{(S13)}$$

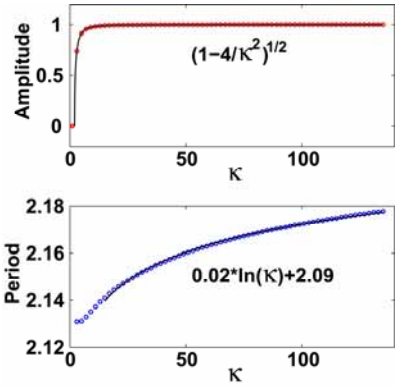

Figure S-IV: Amplitude (upper) and period (lower) for various κ values Circles are given by numerical simulations and solid lines are Eq. (S13) and the least square fitting by using a logarithmic function of κ (Eq. (S12)).

suggesting that the amplitude increases as κ (>2) increases and has an upper limit as shown in Fig. S-IV.

References

1. J. Lewis, *Curr Biol* **13**, 1398 (2003).

Representative simulation parameter values. Oscillation is robust to changes in parameter values.

Parameter	**Value (unit)**	**Meaning**
a	0.5 (molecules/min)	Production rate for mRNA
b, c	0.11 (1/min)	Degradation rate for NICD, mRNA, and protein
p_0	13 (min)	Gain value of Hes7 for inhibition of protein production
T_p	15 (min)	Time delay for mRNA nuclear export and protein production
T_m	20 (min)	Time delay for Hes7 nuclear imports

Supplementary Note 2

Statistical analysis of somite number

1 Outline

To statistically evaluate the difference in the average somite number between two genotypes *Nrarp*$^{-/-}$ and *Nrarp*$^{+/+}$, a paired t-test was first performed; the difference was not significant for E 8.5, while it was statistically significant for E 10.5 (p<0.02) and E 11.5 (p<0.01). Next, to evaluate the statistical difference in terms of inference, such as the confidence interval (CI), we developed a generative model that simulates the statistical generation process of somite number of each embryo. This model includes a parameter m_t that represents the mean genetic effect of a somite number decrease in genotype t=*Nrarp*$^{-/-}$ relative to the number of somites in t=*Nrarp*$^{+/+}$. A 95% CI of the extension in the segmentation clock period was estimated after obtaining a 95% CI of the parameter m_t by applying statistical inference to the generative model.

Note that overall statistical significance was evaluated with the simple paired t-test, and the parameters were then estimated to further examine the physical meaning of the significance, if any. In the following, we define the generative model to evaluate the parameters and describe the inference technique we used.

2 Generative model

It is assumed that the somite number of each litter obeys the following generative model:

$$x_i = \mu_{l(i)} + m_{t(i)} + \varepsilon_i \qquad (1)$$

where x_i , $\mu_{l(i)}$, $m_{t(i)}$, and ε_i denote somite number of the i-th litter, mean somite number of wild-type littermates in the $l(i)$-th pregnant female, mean increase in the somite number of the $t(i)$-th genotype, and noise effect (variation) of an individual litter i, respectively. l=$l(i)$ signifies the pregnant female that conceived the i-th litter, and t=$t(i)$ signifies the genotype which the i-th litter belongs to; t=0 and t=1 denote wild type (+/+) and homo type (-/-), respectively. Since the mean increase m_t is a relative one from the wild type's somite number, m_0=0 holds.

It is natural to assume there are two factors leading to the statistical variation in the somite number: a pregnant female-dependent one and an individual litter-dependent one. To dissociate these factors, μ_l and ε_i are assumed to be generated by the following hierarchical model:

$\mu_l \sim N(\mu_{E(l)}, \sigma_\mu^2)$, (2)

$\varepsilon_i \sim N(0, \sigma^2)$, (3)

where $\mu_{E(l)}$, σ_μ^2, and σ^2 are unknown parameters to be estimated. $a \sim N(b, c^2)$ denotes that a obeys Gaussian distribution of mean b and variance c^2. $E=E(l)$ denotes the epoch of the l-th processed pregnant female, either E 8.5, E 10.5, or E 11.5.

The parameters of the model should be estimated somehow on the basis of observation; somite number x_i is observed for each litter. The parameters are divided into three categories: (a) parameters $\mu_{E(l)}$, σ_μ^2 and σ^2 are point estimated by using the maximum likelihood method; (b) parameter μ_l is not estimated, because it is integrated out; and (c) parameter m_1 is estimated as a 95% confidence interval (CI).

Since equations (1), (2), and (3) define the likelihood function of the parameters, after integrating (marginalized) the likelihood function with respect to μ_l ((b)-type), the (a)-type parameters are estimated so as to maximize the marginalized likelihood, and CI of m_1 ((c)-type) is also obtained.

3 Parameter estimation results

The observed data are summarized in Table S5, and the parameters estimated from them are shown in Table S6.

Table S5. Statistics of somite number data.

Processing epoch	num. of pregnants	num. of *Nrarp*$^{+/+}$ litters	num. of *Nrarp*$^{-/-}$ litters
E8.5	6	19	19
E10.5	18	49	69
E11.5	8	25	25

Table S6. Model estimation results.

Processing epoch	95% CI of m_1	μ_E	σ_μ	σ
E8.5	(-1.02, 0.51)	12.37	2.21	1.17
E10.5	(-0.92, -0.12)	39.67	3.38	1.09
E11.5	(-2.65, -1.10)	52.77	2.02	1.33

The 95% CI of m_1 in table S6 is consistent with the result of the paired t-test, since the CI for E 8.5 includes zero while those for E 10.5 and E 11.5 do not. The estimate of μ_E, the average of mean somite number in the pregnant females, was slightly different from the average somite numbers of wild type litters, though the difference was negligible. The smaller estimated standard deviation σ_μ than σ implies that a high genetic relevance can be found even though there is a large variation in somite number between different pregnant females.

We transformed the 95% CI (-2.6, -1.1) of m_1 into that of the mean segmentation clock period. The average increase in somite number in 72 hours between E 8.5 and E 11.5 is $\mu_{E11.5}$-$\mu_{E8.5}$=40.4 in the wild type litter. The 95% CI of the increase in somites in the homo-*Nrarp*-loss type within the same 72 hours is (37.7, 39.3). Assuming a uniform somite generation process during the 72 hours between E 8.5 and E 11.5, the 95% CI of the segmentation clock period extension during the 72 hours is estimated to be (3.0, 7.5) minutes.